Titre: Title:	Mechanical behavior of iron ore tailings under standard compression and extension triaxial stress paths
Auteurs: Authors:	Alexia Cindy Wagner, João Paulo de Sousa Silva, João Vítor de Azambuja Carvalho, Ana Luisa Cezar Rissoli, Pedro Cacciari, Helder Mansur Chaves, Hugo Carlos Scheuermann Filho, & Nilo Cesar Consoli
Date:	2023
Type:	Article de revue / Article
Référence: Citation:	Wagner, A. C., Silva, J. P. S., Carvalho, J. V. A., Rissoli, A. L. C., Cacciari, P., Chaves, H. M., Filho, H. C. S., & Consoli, N. C. (2023). Mechanical behavior of iron ore tailings under standard compression and extension triaxial stress paths. Journal of Rock Mechanics and Geotechnical Engineering, 15(7), 1883-1894. https://doi.org/10.1016/j.jrmge.2022.11.013

Titre de la revue: Journal Title:	Journal of Rock Mechanics and Geotechnical Engineering (vol. 15, no. 7)
Maison d'édition: Publisher:	Elsevier
URL officiel: Official URL:	https://doi.org/10.1016/j.jrmge.2022.11.013
Mention légale: Legal notice:	© 2023 Institute of Rock and Soil Mechanics, Chinese Academy of Sciences. Production and hosting by Elsevier B.V. This is an open access article under the CC BY license (http://creativecommons.org/licenses/ by/4.0/).

Journal of Rock Mechanics and Geotechnical Engineering 15 (2023) 1883–1894

Contents lists available at ScienceDirect

Journal of Rock Mechanics and Geotechnical Engineering

journal homepage: www.jrmge.cn

Full Length Article

Mechanical behavior of iron ore tailings under standard compression and extension triaxial stress paths

Alexia Cindy Wagner [a], João Paulo de Sousa Silva [b], João Vítor de Azambuja Carvalho [a], Ana Luisa Cezar Rissoli [b], Pedro Pazzoto Cacciari [b,c], Helder Mansur Chaves [a], Hugo Carlos Scheuermann Filho [a], Nilo Cesar Consoli [a,*]

[a] Universidade Federal do Rio Grande do Sul, Porto Alegre, 90035-190, Brazil
[b] Mineral Development Centre, Vale S.A., Santa Luzia, 33040-900, Brazil
[c] Department of Civil, Geological and Mining Engineering, Polytechnique Montreal, Montreal, H3C 3A7, Canada

ARTICLE INFO

Article history:
Received 17 June 2022
Received in revised form
13 October 2022
Accepted 14 November 2022
Available online 17 December 2022

Keywords:
Iron ore tailings (IOTs)
Dry stacking
Critical state soil mechanics
Extension tests
Stress path

ABSTRACT

The disposal of mining tailings has increasingly focused on the use of dry stacks. These structures offer more security since they use filtered and compacted material. Because of the construction method and the heights achieved, the material that compounds the structure can be subjected to different stress paths along the failure plane. The theoretical framework considered in the design of these structures generally is the critical state soil mechanics (CSSM). However, the data in the literature concerning the uniqueness of critical state line (CSL) is still controversial as the soil is subjected to different stress paths. With respect to tailings, this question is even more restricted. This paper studies two tailings with different gradings due to the beneficial processes over extension and compression paths. A series of drained and undrained triaxial tests was conducted over a range of initial densities and stress levels. In the q-p' plane, different critical stress ratio (M) values were obtained for compression and extension stress paths. However, the critical state friction angle is very similar with a slightly higher critical state friction angle for extension tests. Curved stress path dependent CSLs were obtained in the v-lnp' plane with the extension tests below the CSL defined in compression. Regarding the fines content, the studied tailings presented very similar M and critical state friction angle values. However, the fines content affects the volumetric behavior of the studied tailings and the CSLs on the v-lnp' plane shift downwards with the increasing fines content for compression and extension tests. In relation to dilatancy analysis, the fines content did not present an evident influence on the dilatancy of the materials. However, different values of mean stress ratio N were obtained between compression and extension tests and can corroborate the existence of non-unique CSLs for these materials.

1. Introduction

The laboratory practice in geotechnical engineering usually relies on conventional drained and undrained triaxial compression tests to derive the mechanical response of geomaterials. The generalization to other stress conditions is then achieved by limited sets of different stress paths or in conjunction with some tests performed in other equipment such as the simple shear, hollow cylinder, true triaxial, among others. However, the conditions often found in field can be highly different from those imposed in conventional triaxial compression tests.

One method for disposing tailings (by-product from ore extraction) is using dry stacks. In this construction method, the stack compounding materials can be subjected to different conditions. To build these structures, the tailings are filtered to low moisture content and compacted to a specified compaction energy. Different compaction levels are attributed to different regions of the dry stacking. Structural zone exists at the borders of the stack, where the material is compacted in denser states, while internally it can be deposited in looser conditions in the stack (Davies, 2011; Lupo and Hall, 2011).

* Corresponding author.
E-mail address: consoli@ufrgs.br (N.C. Consoli).
Peer review under responsibility of Institute of Rock and Soil Mechanics, Chinese Academy of Sciences.

https://doi.org/10.1016/j.jrmge.2022.11.013

The material at the borders, if analyzed by a curved failure plane, can be subjected to different stress paths along this failure plane (Fig. 1). The shear mode could vary from compression just at the center to extension near the toe. Fotovvat and Sadrekarimi (2022) suggested the different stress paths that the material can be subjected to during the construction of an embankment. Initially, sediments are anisotropically consolidated in compression with different shear modes along a possible failure plane. The stress condition may change during the raising of the embankment, subjecting the material to new stress paths. Nevertheless, further expansion of the embankment could reverse the initial loading direction and submit the material to a new set of consolidation and shear paths.

The theoretical framework, usually considered in the design of these structures, that accounts for the influence of stresses and density in the state of granular materials is the critical state soil mechanics (CSSM) (Schofield and Wroth, 1968). Thus, the need for predicting soil behavior at different stress paths and the use of CSSM for this give rise to doubts concerning the uniqueness of the critical state line (CSL). This is still controversial, as the data in the literature argue for and against the uniqueness of CSL because of different factors.

Regarding the stress path to which the material is subjected, there are both experimental (Been et al., 1991; Verdugo and Ishihara, 1996; Li et al., 2013; Schnaid et al., 2013) and numerical (Li and Dafalias, 2012; Zhao and Guo, 2013; Gao et al., 2014) studies supporting the uniqueness of CSL as well as the non-uniqueness (Riemer and Seed, 1997; Huang et al., 2014; Salvatore et al., 2017; Kodicherla et al., 2021; Fotovvat and Sadrekarimi, 2022). Most of the work reported in the literature, however, is based on tests on uniform clean sands.

Schnaid et al. (2013) presented an experimental program for tailings from a gold mine which comprised the realization of few triaxial extension tests that fall in the same CSL defined from triaxial compression tests. On the other hand, Fotovvat and Sadrekarimi (2022) presented for the tailings of another gold mine a study with six different stress paths which fall in two different CSLs related to their shear mode, consolidation path and liquefaction behavior.

An experimental program comprising drained and undrained triaxial tests in both compression and extension with different consolidation paths for two types of iron ore tailings (IOTs) is presented herein. Tailings are a mix of fines and granular particles. Different gradings of tailings can be obtained in the same iron ore beneficiation plants due to the difference in ore quality or to different stages of ore processing. Therefore, it is important to learn the influence of minor changes in grading on the overall behavior of the tailings. The study aims to address the influence of fines content on the uniqueness of CSL in compression and extension loading paths of IOTs. The stress–strain response for both tailings at the different stress paths is also evaluated. A dilatancy analysis of compression and extension tests on IOTs is presented to enhance the discussion of strain mechanisms for tailings previously reported in the literature. Also, some insights are presented in reference to the importance of deformation direction on volumetric behavior of tailings subjected to different stress paths.

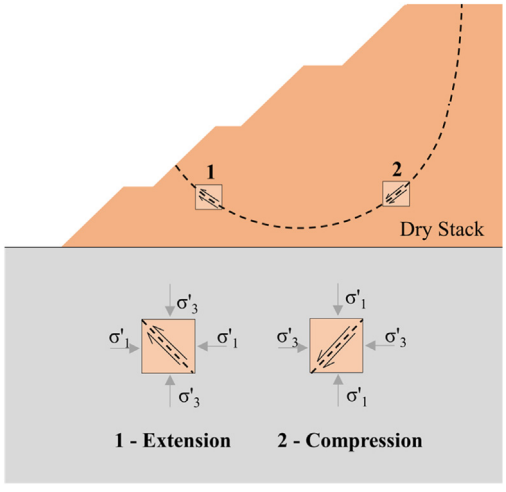

Fig. 1. Shear modes in dry stack.

Fig. 2. Location of the Quadrilátero Ferrífero in the province of Minas Gerais, Brazil.

2. Experimental program

The experimental program consists of 24 triaxial compression tests and 12 triaxial extension tests. Also, the physical characteristics of the two IOTs were determined.

2.1. Materials

The IOTs studied are from Quadrilátero Ferrífero located in the province of Minas Gerais, Brazil (Fig. 2). This region produces approximately 200 million tons of iron ore per year and is responsible for approximately 40% of all Brazilian iron ore production. The activities involved in mining and processing iron ore include crushing and screening methods to more sophisticated processes to upgrade the ore quality. The two IOTs analyzed in this study show different gradings due to different beneficiation stages. The IOT specimens were collected at different exit points of iron ore beneficiation plants. Both tailings are by-products of iron ore processing. The finer tailings (S1) are removed from the production chain earlier than the coarser tailings (S2) because the presence of fines makes it difficult to retrieve the iron from the ore by the flotation process. Therefore, the S1 tailings are obtained before the flotation process and the S2 tailings are obtained after the flotation process.

Fig. 3 depicts the grain size distributions of the finer tailings (S1) and coarser tailings (S2). The particle size distribution was obtained following ASTM D7928–21e1 (2021a) and the specific gravity was evaluated according to ASTM D854–14 (2014). The Atterberg limits were evaluated according to ASTM D4318–17e1 (2017a) and both tailings are non-plastic. Both tailings are classified as silty sand (SM) in accordance with the Unified Soil Classification System

(ASTM D2487–17e1, 2017b). The compaction characteristics were assessed using both the standard and modified efforts in agreement with ASTM D698–12 (2021b) and ASTM D1557–12 (2021c), as shown in Fig. 4. The compaction curves present different patterns of behavior. For the S1 tailings, the optimum moisture content was reduced with increasing energy, as was expected. However, for the S2 tailings, this difference was smaller. Furthermore, the S1 tailings presented a more pronounced peak of dry specific weight, possibly because the moisture content variation caused a marked change in specimen structure. This indicates that the particle shape and size of the tailings influence the behavior of the material to be compacted at different moisture contents.

The differences in the physical properties of the two tailings are associated with their production process. The S1 tailings have a fines content (*FC*) of 52.2% and a specific weight (G_s) of 3.05. The S2 tailings have a fines content (*FC*) of 33.3% and a specific weight (G_s) of 2.97. This feature is associated with the process of iron ore beneficiation for the different tailings. When there are more fines in the tailings, iron recovery becomes more difficult and consequently, the iron content and specific weight of this material will be higher. The results of the mineralogy analysis are shown in Fig. 5. These results were obtained by an associated analysis of scanning electron microscope (SEM) with energy dispersive spectroscopy (SEM-EDS), which has enabled the quantification of the mineral phases. Mineralogically, the IOTs are mainly constituted by quartz and iron oxide, amongst other minor crystals. The S1 tailings present 76.2% of quartz and 20.9% of iron oxide, while the S2 tailings present 78.4% of quartz and 17.2% of iron oxide. Although the phases are very similar, the finer material has a slightly higher iron content, which is as expected.

SEM images of both tailings are presented in Fig. 6. The SEM images showed that iron tailings consist of two types of main elements: bulky particles (large, subangular and subrounded shape) and flocks (collections of clay-sized particles). These elements exist in different quantities and the particle size range varies for the two tailings. The S1 tailings contain higher amounts of bulky particles surrounded by flocks, while S2 tailings contain higher quantities of

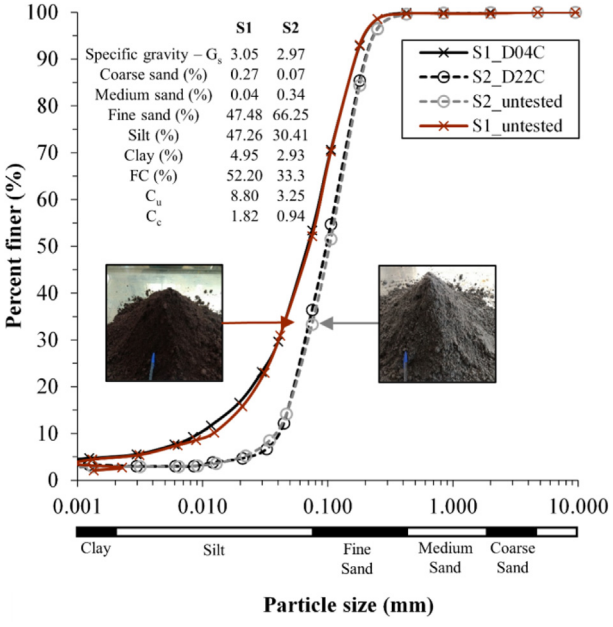

Fig. 3. Grain size distribution for untested and tested tailings.

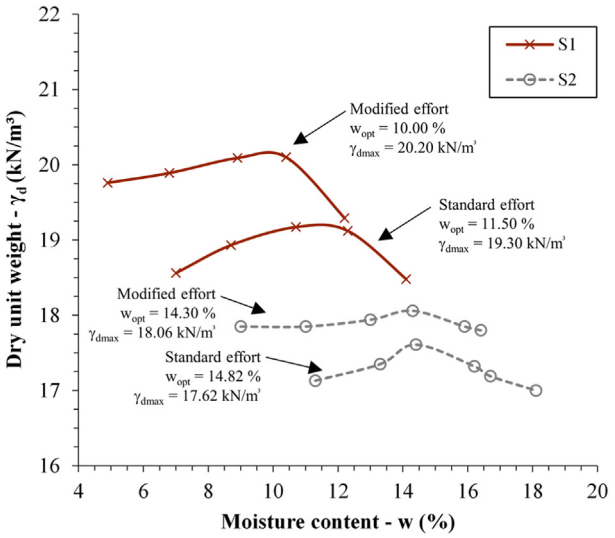

Fig. 4. Compaction characteristics of tailings.

bulky particles. The existence of fines among the coarser particles can influence the geotechnical behavior of the materials, and this characteristic will be investigated in the paper.

Based on this, it is possible to relate the differences observed in compaction behavior to the mineralogical origin of tailings and the presence of smaller particles in the granular matrix. The fines present in the S1 tailings induced a fabric in compaction in which the smaller particles surround the greater ones. Thus, the specimens achieve a more compacted state with more contacts and fewer voids. However, for the S2 tailings, this difference is not much marked and may be related to a more common origin with quartzitic particles being the main constituent of the mineral matrix. The moisture content has more influence on the S1 tailings (compaction curve with more pronounced peak) because it can change the fabric (fine particles sliding in different ways depending on water content and creating different arrangements with the largest particles).

2.2. Methods

2.2.1. Specimen molding

Cylindrical specimens were molded through moist tamping (Ladd, 1978; Frost and Park, 2003; Corrêa and Oliveira Filho, 2019) in different compaction levels with 50 mm in diameter and 100 mm in height. Six layers were used in this process, with the first, second, third, fourth and fifth layers being scarified at the top to guarantee the adherence of the subsequent layer. Based on the results depicted in Fig. 4, a single moisture content (w) of 10% was chosen irrespective of the adopted dry unit weight.

2.2.2. Triaxial tests

A series of triaxial tests was performed to evaluate the stress–strain response and the differences of the two materials in compression plane (v-lnp', where $v = 1 + e$ is the specific volume, e is the void ratio, and p' is the mean effective stress). Conventional isotropically consolidated drained (CID) and undrained (CIU) triaxial compression tests and K-consolidated undrained (CKUE) and drained (CKDE) triaxial extension tests were undertaken to assess the differences in the mechanical response and CSL caused by the different effective stress paths followed. Furthermore, the

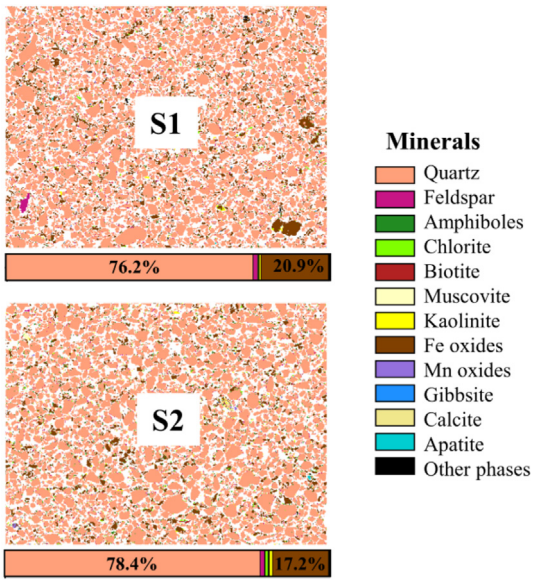

Fig. 5. Mineralogy analysis.

adoption of these effective stress paths had the intention to simulate the states that the materials may experience in field.

All the tests were performed on fully saturated specimens following the recommendations of ASTM D7181–20 (2020a) and ASTM D4767–11(2020) (2020b). The saturation process consisted of water percolation and application of back-pressure increments until a *B*-value greater than 0.98 was obtained. In addition, the P-wave velocity (V_p) was measured after the saturation process was finished and the values obtained were greater than 1500 m/s in all cases, which is associated with the specimen's full saturation (e.g. Viana da Fonseca et al., 2021). The dry stacks usually are built in an unsaturated state. However, the rainfall and water infiltration throughout their life cycle can result in total saturation of the material. Therefore, saturated tests represent the behavior of the tailings in its most critical situation, in which there is no contribution of the additional strength caused by matric suction generated in unsaturated porous media.

In triaxial compression tests, the isotropic consolidation was carried out at a constant rate of 50 kPa/h up to the desired pressure. Then, the strain-controlled shearing was executed at a rate of 1.5 mm/h. Regarding the triaxial extension tests, consolidation phase was carried out with *K* of 0.7 and shear phase was strain-controlled, with the horizontal stress (σ'_h) kept constant and the axial stress (σ'_a) relieved at a rate of 1.5 mm/h. The setup used for the extension tests was same as that adopted for compression tests with the difference that a suction cap was used to enable the vertical unloading of the specimen.

End-of-test soil freezing technique (Sladen and Handford, 1987; Viana da Fonseca et al., 2021) was used in all cases to estimate the

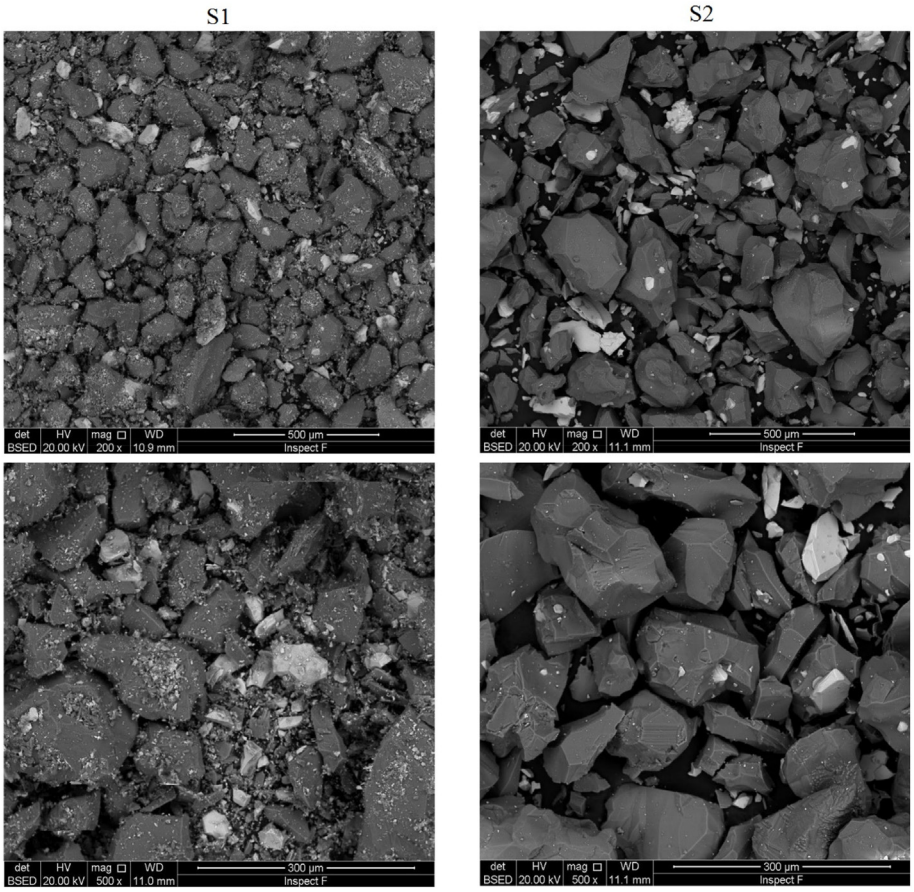

Fig. 6. SEM images of tailings.

void ratio achieved after shearing of the specimens. Table 1 summarizes the experimental program conducted.

3. Results

3.1. Stress–strain behavior in compression tests

Seven drained triaxial compression tests were performed at confining pressures between 100 kPa and 1600 kPa for each material with different initial densities. The stress–strain response and the volumetric change behavior in triaxial compression under drained conditions are presented in Fig. 7. The loosest specimens have shown a ductile response accompanied by a fully contractive behavior. The denser specimens have a stiffer stress–strain curve with a slight peak strength associated with an initial contractive response followed by a dilative trend. Fig. 7 also indicates that most specimens tend to have stability in volumetric strains and deviatoric stress with increasing axial strain and this was considered in the critical state analysis. It is observed that the drained compression behavior is similar for both tailings studied.

Fig. 8 presents the stress–strain and pore pressure change responses of the IOTs sheared under undrained compression condition. Five undrained triaxial compression tests were performed at confining pressures from 400 kPa to 1600 kPa for each material with different initial densities. In general, it is verified that the undrained compression behavior is also similar for the different tailings. A significant loss of strength has taken place in the loosest specimens at lower confinement levels due to positive pore pressure generation. This was accompanied by a strain-softening response and indicates susceptibility to static liquefaction. The denser specimens have shown an initial positive pore pressure variation which then turned into a negative pore pressure change. This behavior was associated with a strain-hardening stress–strain response which is more marked in S1 specimen, with specimen S2 showing a tendency of stabilization for pore pressure change and deviatoric stress.

3.2. Stress–strain response in extension tests

The results of the drained and undrained extension tests are depicted in Fig. 9a and b, respectively. The tests were performed at confining pressures of 300 kPa, 600 kPa and 1200 kPa for each material in an initial dense state. The specimens of the two tailings show a similar response under drained and undrained shearing. Regarding the volumetric behavior, there was an initial compression followed by a dilatative trend for the drained tests and a tendency for the pore pressure to increase firstly and then decrease in the undrained tests. With respect to the stress–strain behavior, a strain-hardening behavior was noticed in the undrained tests and no tendency to static-liquefaction was found. For the drained tests, the deviatoric stress tends to stabilize. Unfortunately, larger axial strains could not be achieved in the extension tests due to equipment limitations to this stress path.

Table 1
Test summary.

ID	Material	Drainage	Consolidation	p'_0 (kPa)	Type	v_i	Ψ	Initial state	End of shearing		
									v	p' (kPa)	q (kPa)
S1_D01C	S1	Drained	Isotropic	200	Compression	1.75	0.076	Wet	1.65	378.78	538.32
S1_D02C	S1	Drained	Isotropic	400	Compression	1.73	0.075	Wet	1.62	757.91	1075.99
S1_D03C	S1	Drained	Isotropic	800	Compression	1.7	0.077	Wet	1.59	1507.39	2119.7
S1_D04C	S1	Drained	Isotropic	1600	Compression	1.65	0.075	Wet	1.54	3000.04	4196.65
S1_D05C	S1	Drained	Isotropic	100	Compression	1.68	−0.016	Dry	1.68	186.52	256.55
S1_D06C	S1	Drained	Isotropic	300	Compression	1.66	−0.004	Dry	1.65	564.05	789.16
S1_D07C	S1	Drained	Isotropic	900	Compression	1.52	−0.098	Dry	1.55	1774.76	2618.27
S1_U08C	S1	Undrained	Isotropic	400	Compression	1.73	0.072	Wet	1.73	9.53	16.51
S1_U09C	S1	Undrained	Isotropic	800	Compression	1.69	0.07	Wet	1.69	44.15	66.73
S1_U10C	S1	Undrained	Isotropic	400	Compression	1.58	−0.079	Dry	1.58	1135.06	1589.02
S1_U11C	S1	Undrained	Isotropic	800	Compression	1.58	−0.046	Dry	1.58	1540.73	2065.18
S1_U12C	S1	Undrained	Isotropic	1600	Compression	1.55	−0.027	Dry	1.55	2221.98	3128.85
S1_D13E	S1	Drained	*K*	300	Extension	1.56	[a]	Dry	1.56	200.57	−186.97
S1_D14E	S1	Drained	*K*	600	Extension	1.55	[a]	Dry	1.55	389.15	−407.54
S1_D15E	S1	Drained	*K*	1200	Extension	1.55	[a]	Dry	1.54	790.21	−779.59
S1_U16E	S1	Undrained	*K*	300	Extension	1.57	[a]	Dry	1.57	389.92	−393.92
S1_U17E	S1	Undrained	*K*	600	Extension	1.54	[a]	Dry	1.54	542.21	−539.03
S1_U18E	S1	Undrained	*K*	1200	Extension	1.55	[a]	Dry	1.55	707.72	−673.59
S2_D19C	S2	Drained	Isotropic	200	Compression	1.88	0.085	Wet	1.79	375.77	527.99
S2_D20C	S2	Drained	Isotropic	400	Compression	1.85	0.075	Wet	1.75	742.02	1021.62
S2_D21C	S2	Drained	Isotropic	800	Compression	1.84	0.1	Wet	1.71	1460.94	1977.88
S2_D22C	S2	Drained	Isotropic	1600	Compression	1.81	0.113	Wet	1.64	2901.76	3905.62
S2_D23C	S2	Drained	Isotropic	100	Compression	1.75	−0.066	Dry	1.79	166.36	196.08
S2_D24C	S2	Drained	Isotropic	300	Compression	1.75	−0.037	Dry	1.77	533.28	693.83
S2_D25C	S2	Drained	Isotropic	900	Compression	1.75	0.01	Wet	1.72	1625.14	2172.42
S2_U26C	S2	Undrained	Isotropic	400	Compression	1.85	0.075	Wet	1.85	0	0
S2_U27C	S2	Undrained	Isotropic	800	Compression	1.82	0.075	Wet	1.82	101.33	140.41
S2_U28C	S2	Undrained	Isotropic	400	Compression	1.69	−0.086	Dry	1.69	1256.55	1635.72
S2_U29C	S2	Undrained	Isotropic	800	Compression	1.68	−0.068	Dry	1.68	1724.83	2242.54
S2_U30C	S2	Undrained	Isotropic	1600	Compression	1.66	−0.041	Dry	1.66	2183.02	2870.3
S2_D31E	S2	Drained	*K*	300	Extension	1.68	[a]	Dry	1.69	202.17	−182.89
S2_D32E	S2	Drained	*K*	600	Extension	1.69	[a]	Dry	1.69	396.21	−387.15
S2_D33E	S2	Drained	*K*	1200	Extension	1.64	[a]	Dry	1.64	801.53	−746.60
S2_U34E	S2	Undrained	*K*	300	Extension	1.68	[a]	Dry	1.68	413.89	−408.39
S2_U35E	S2	Undrained	*K*	600	Extension	1.66	[a]	Dry	1.66	645.92	−697.75
S2_U36E	S2	Undrained	*K*	1200	Extension	1.65	[a]	Dry	1.65	711.72	−662.53

[a] The state parameter Ψ is not presented because a reliable CSL for the extension tests could not be determined. v_i is the specific volume before shearing; p'_0 is the mean effective stress at the beginning of the shearing; and $q = \sigma_1 - \sigma_3$ is the deviatoric stress, where σ_1 and σ_3 are the major and minor principal stresses, respectively.

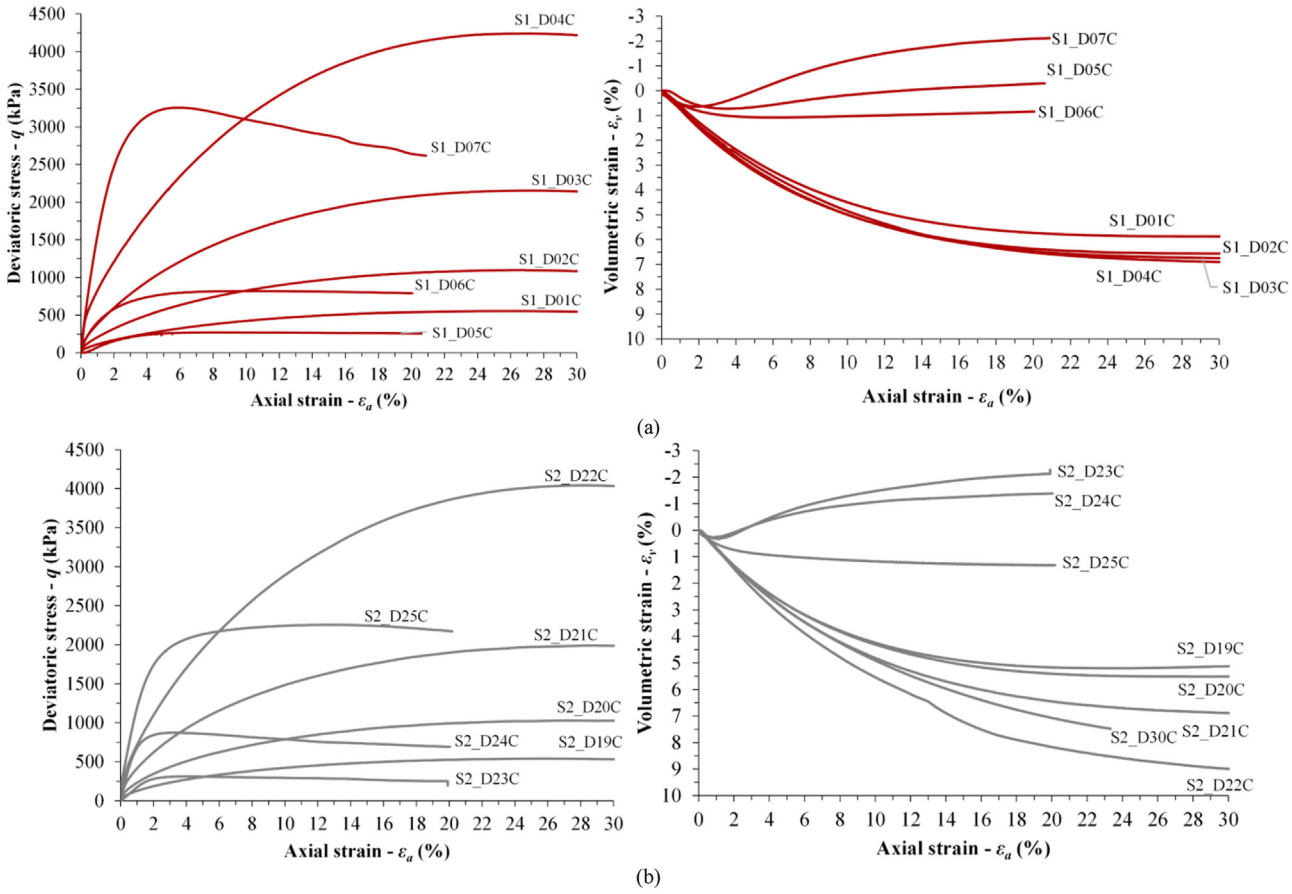

Fig. 7. Stress–strain behavior of (a) S1 and (b) S2 in drained compression tests.

3.3. Critical state analysis

3.3.1. q-p' plane

The critical state is defined as the state of a granular media, achieved by shearing, in which it deforms in the absence of variations of volume, deviatoric stress, and mean normal effective stress (Schofield and Wroth, 1968; Atkinson, 2007). The locus of the critical state is defined by a surface in v-p'-q space and is usually analyzed in the derived v-lnp' and q-p' planes. The stress–strain results for compression and extension stress paths are plotted in q-p' space in Fig. 10 for both tailings studied.

In this space, for the stresses achieved, the trace of CSL can be represented by a straight line for both compression and extension, with slopes of M_c and M_e, respectively. The CSL slope (M) in q-p' is known to vary as a function of Lode's angle (θ) that defines the proportion of intermediate principal stress in relation to the major and minor principal stresses. For triaxial compression, θ is equal to 30°, while for triaxial extension, it takes the value of −30°. The variation of M with the intermediate principal stress does not imply that the critical state friction angle varies (Jefferies and Been, 2015).

For the finer tailings in compression (Fig. 10a), a gradient M_c of 1.4 was found, corresponding to a critical state friction angle (φ'_{cs}) of 34.6°, and for extension, values of 0.98 for M_e and 35.8° for φ'_{cs} were obtained. The results for S2 (Fig. 10b) were similar, indicating a slightly smaller critical state friction angle for compression tests (33.4°), as well as for extension tests (34.8°). These findings also agree with discrete element method (DEM) simulations performed considering an assemblage of elastic spheres (Huang et al., 2014) or clumps (Kodicherla et al., 2021) and with experimental data from literature (Matsuoka and Nakai, 1974; Yamamuro and Lade, 1996). The higher strength experimentally verified in the triaxial extension tests may be attributed to an increased stiffness in the direction of axial strains caused by the direction of compaction imposed during the molding of the specimens.

Regarding the fines content, the tailings studied presented similar values for φ'_{cs} with the finer material presenting slightly higher strength in both compression and extension. The evolution of stress ratio η ($\eta = q/p'$) during shearing for both tailings in compression and extension is depicted in Fig. 11. The results reaffirm the observed similarity in the behavior of the materials, indicating that the same mechanisms control strength in both cases. The values obtained for critical state friction angle, irrespective of stress path followed, are in the usual range of values for tailings presented by Li et al. (2018).

3.3.2. Dilatancy analysis

A stress–dilatancy analysis was carried out for the drained compression and extension tests by plotting the stress ratio η as a function of the dilation rate ($D = d\varepsilon_v/d\varepsilon_s$) in Fig. 12. The outcomes have shown the behavior of a typical purely frictional material where the peak strengths are associated with dilation. It is observed that all tests (loose and dense specimens) tend towards the same critical state stress ratio value as shearing develops (the respective M-values previously presented).

Concerning the volume change response, all the looser specimens have presented a contractive behavior during the shearing while the denser specimens have dilated after an initial compression. The tests with dilative behavior are represented by a value of

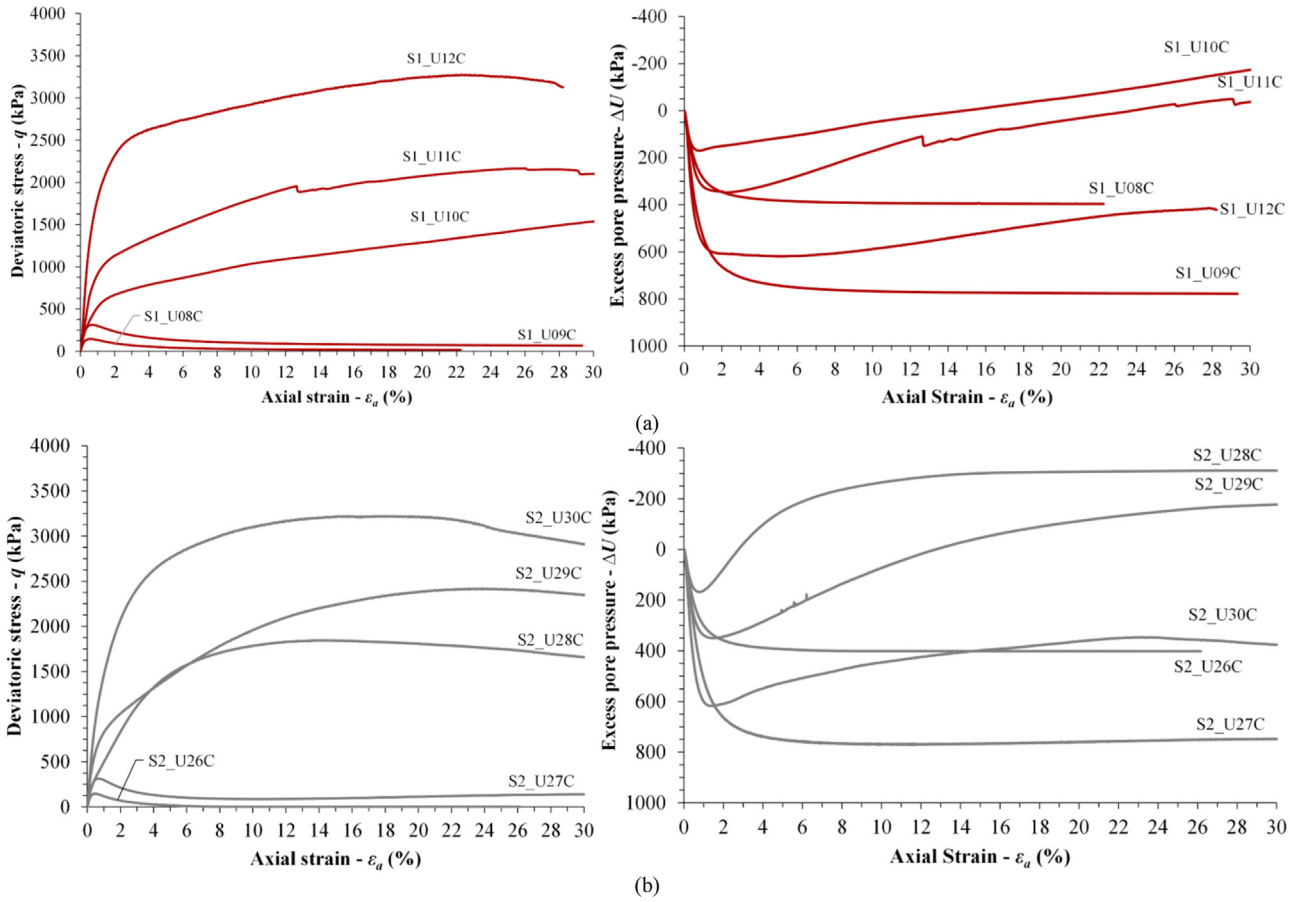

Fig. 8. Stress–strain behavior of (a) S1 and (b) S2 in undrained compression tests.

measured dilatancy D_{min} at peak strength η_{max}. Fig. 13a depicts the points plotted for different stress paths and materials. It is observed that the maximum stress ratio (η_{max}) is proportional to the maximum dilatancy (D_{min}) in all cases, and a linear equation can fit it. Also, it is possible to confirm the M_c (or M_e) value defined by taking the intercept of stress ratio axis at zero dilatancy. The behavior of the curves is very similar, and different gradient values do not provide accurate trends because the typical scattering due to few tests might influence them.

It is difficult to establish a relationship between the dilatancy and index properties due to the lack of well-defined stress–dilatancy framework. Looking at the tests in Fig. 13a, it is not possible to find an evident influence of the different fines content on the dilatancy of the materials. If there is an influence, this difference is small for both compression and extension tests, and further tests would be required to confirm that.

Then, the compression and extension tests were combined into two single blocks independent of the tailings type to investigate a possible general trend. The results are shown in Fig. 13b. The adjustments obtained resulted in averaged values for M_c and M_e and different slopes for compression and extension lines. According to Jefferies and Shuttle (2002), N controls the mean stress ratio at critical state to that at normal isotropic compression, and this ratio of mean stresses cannot be a function of Lode's angle under the proposition of a unique CSL. Thus, although potential parallelism is seen in the linear adjustments to different stress paths, it is possible to attribute such a difference to non-unique CSLs for these materials. Other authors such as Kodicherla et al. (2021) also found different N-values for compression and extension tests for DEM analysis of granular materials.

3.3.3. v-lnp' plane

The uniqueness of CSL for compression and extension stress paths in the v-lnp' plane is historically a subject of debate (e.g. Mooney et al., 1998; Li and Dafalias, 2012; Kang et al., 2019). Several studies have provided evidence of uniqueness (Been et al., 1991; Schnaid et al., 2013) as well as non-uniqueness (Huang et al., 2014; Fotovvat and Sadrekarimi, 2022). Chu (1995) pointed out that whether there is a unique CSL in the v-lnp' plane, it is a different issue from whether this unique CSL is achievable following a certain stress path. Furthermore, in their experimental program, Fotovvat and Sadrekarimi (2022) achieved different CSLs and related the non-uniqueness to the differences in shear mode, consolidation path, nonuniform void redistribution, and post liquefaction behavior.

On the other hand, Been et al. (1991) achieved a unique CSL through triaxial tests following different stress paths, molding methods, and initial void ratios. The authors suggested that the effects of these variables eventually would be erased with the attainment of large strains. Also, Li and Dafalias (2012) stated by thermodynamic considerations that the uniqueness of CSL would be a requirement in suggesting an anisotropic critical state framework.

The results from the tests conducted in this paper are presented in the v-lnp' plane in Fig. 14. Curved stress path dependent CSLs were obtained for both tailings. Particle size distribution of specimens tested at 1600 kPa of confining stress was evaluated and no

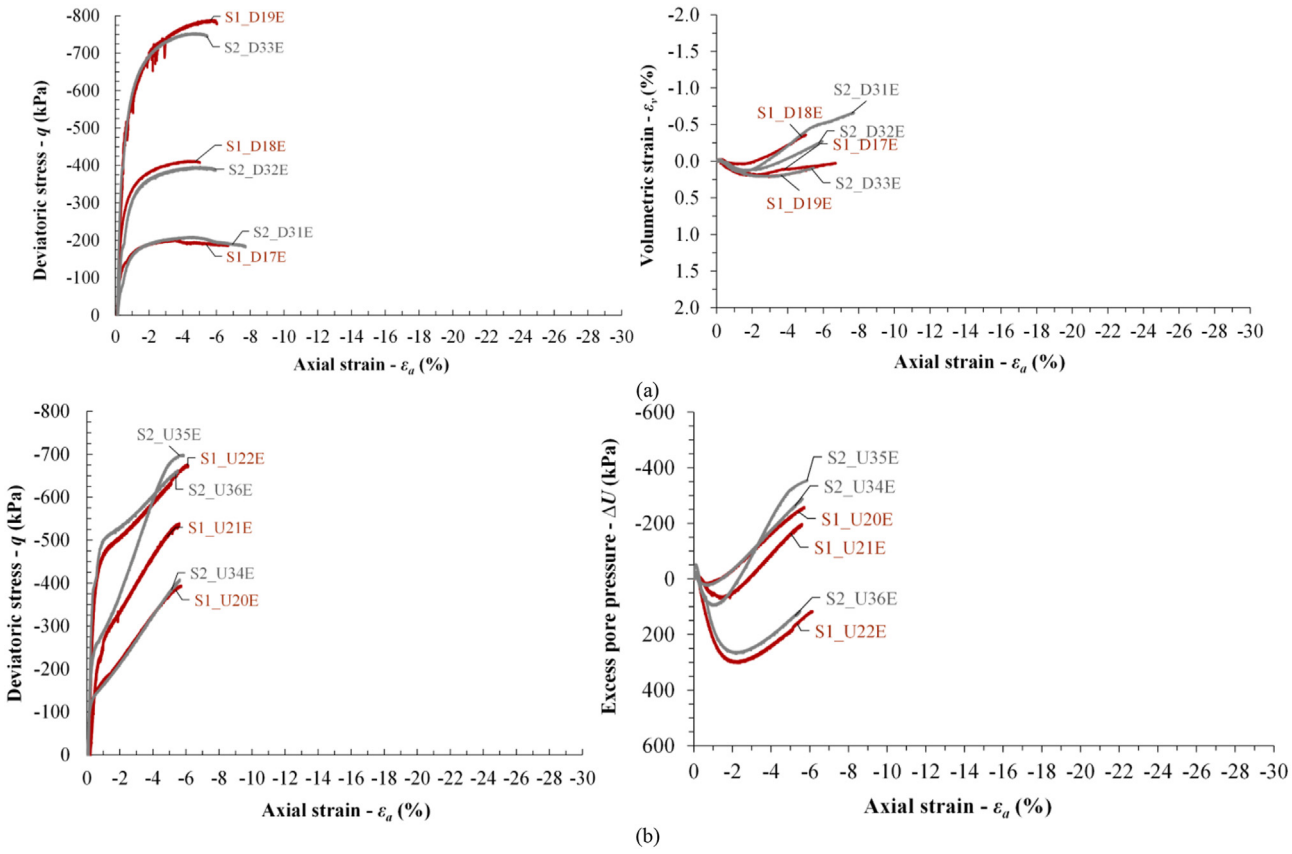

Fig. 9. Stress–strain behavior in (a) drained and (b) undrained extension tests.

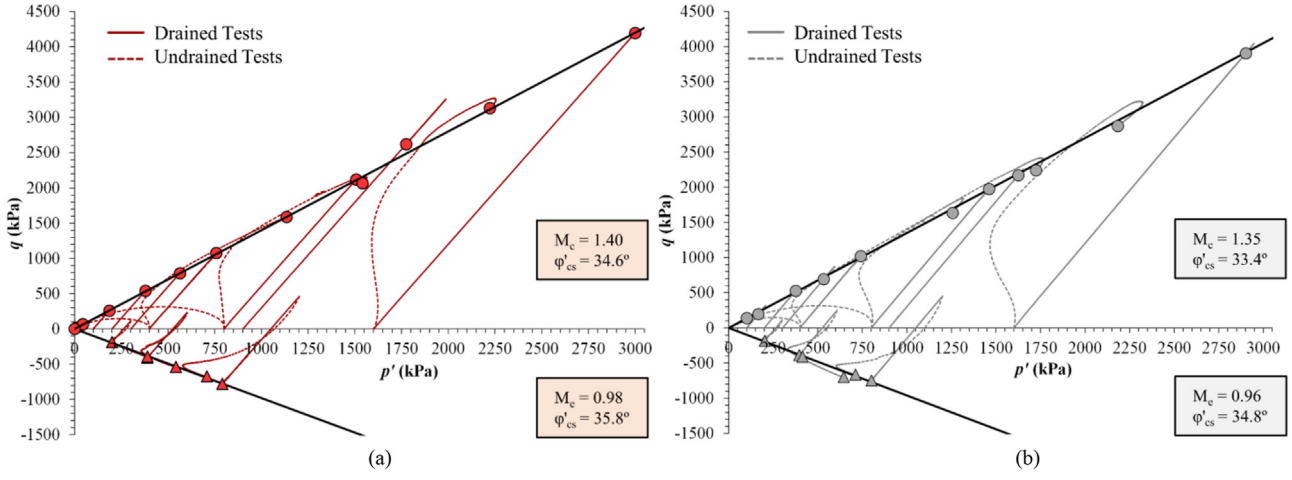

Fig. 10. Stress paths and critical state strength for (a) S1 and (b) S2.

breakage was observed (Fig. 3). Thus, the curved CSLs outlined for both tailings studied are related to the existence of metastable states in which the material can exist at low stresses.

The stability in deviatoric stress, mean effective stress and volumetric strain was considered to determine each of the CSLs. In the case of extension tests, however, it is noted that there are still volumetric strains under the drained conditions, and excess pore pressure under undrained conditions, at the end of the tests. The CSL is then indicated in a region delimited by the directions of the state paths followed by the specimens. Thus, although not precisely determined, the location of CSL for extension tests can be estimated and seems not to converge to the CSL defined for compression tests.

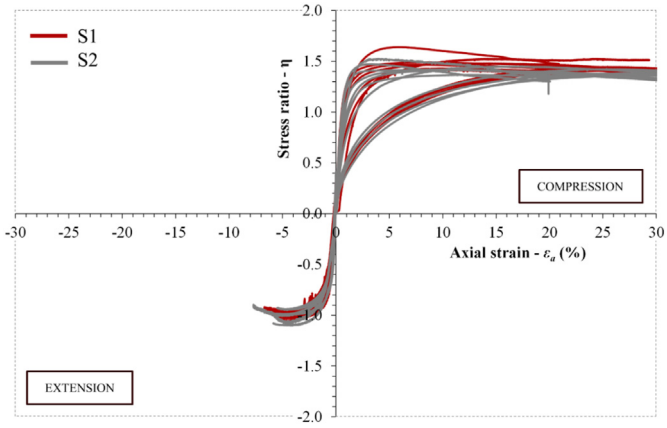

Fig. 11. Stress ratio vs. axial strain for S1 and S2.

The offset from the CSL for compression tests is similar for S1 and S2, with the CSL defined for extension tests below the one defined in compression. These results agree with the findings of Riemer and Seed (1997), Yoshimine et al. (1998) and Salvatore et al. (2017).

Li and Dafalias (2012) pointed out that the anisotropy of the soil behavior and consequently stress path dependency of CSL are due to the preferential orientation of the particle contacts, void spaces, and non-spherical particles. Furthermore, they indicated that the only factor that remains in the large deformations up to the critical state is the non-spherical particles. This condition agrees with the studied tailings since the angular particles (Fig. 6) resulted in different CSLs that depend on the stress path.

Another possible cause for the non-uniqueness in the *v*-ln*p*′ plane is the deformation mode that the specimen is subjected to. Salvatore et al. (2017) found different specimen strain localizations in the compression and extension tests and achieved a unique CSL when they measured the void ratio only on the zones affected by the largest distortion. This indicates that the dependence of the CSL on the stress path occurs when the specimen is considered on a global scale ignoring the strain localization. On the other hand, Riemer and Seed (1997) observed that all specimens subjected to axial compression achieved the same critical state irrespective of the stress path followed, while the specimens subjected to another deformation mode (axial extension or plane strain) converged to a different location. From these results, it is possible to suggest that the position of the CSL in the volumetric plane is more influenced by the strain path than the stress path of the tests. This is supported by the different deformation modes that occur when extending or compressing identical specimens that were molded by axial compaction. In the extension test, the radial strains are more restricted (since the specimen is confined by the major principal stress) while the axial strains tend to develop against the direction of the fabric created by the compaction. This difference in deformations can affect the volumetric behavior of the specimens and consequently the position of the CSL in this plane.

All results are compared in Fig. 15 to investigate the effect of fines content on the extension and compression behavior of the tailings studied. The CSLs in the compression tests appear to be parallel and the adjustment curve shifts downwards with the increasing fines content. Other authors (e.g. Thevanayagam et al., 2002) observed the translation of the curve with change in fines content and defined a “threshold fines content” (TFC). Torres-Cruz and Santamarina (2020) concluded that TFC is approximately 30%. Other authors (Fourie et al., 2001; Thevanayagam et al., 2002; Carrera et al., 2011) found different values of TFC for different granular mixes tested, varying from 40% to 60%. However, the TFC

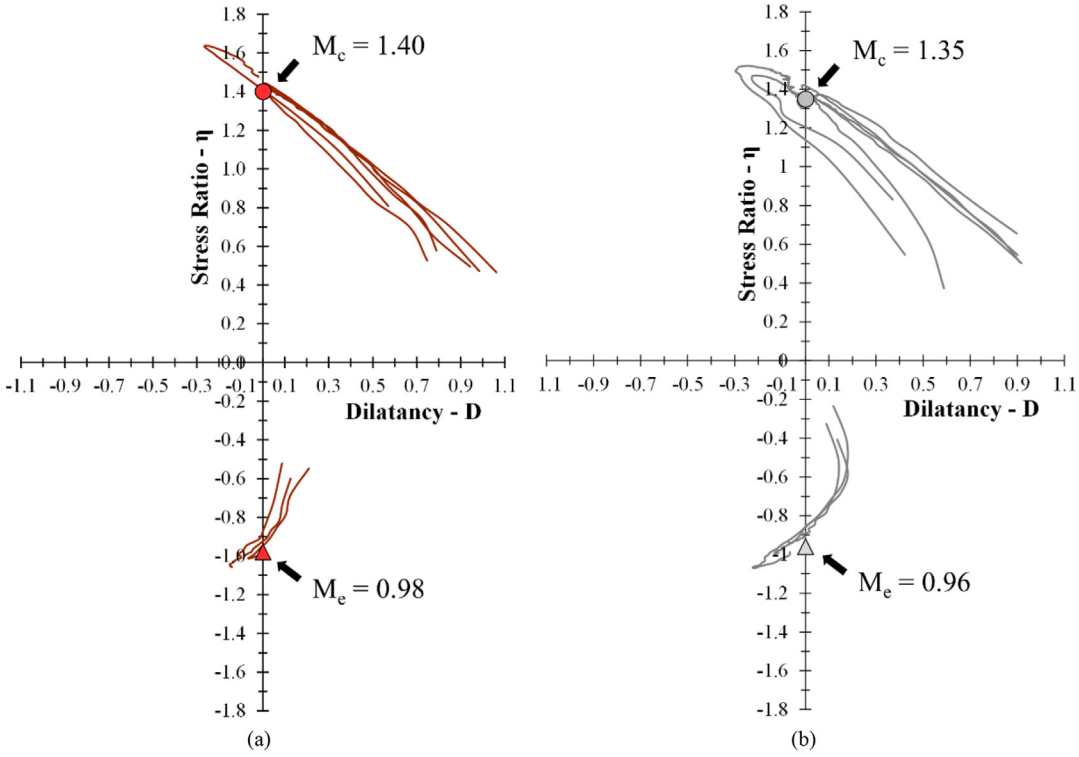

Fig. 12. Stress–dilatancy analysis of (a) S1 and (b) S2.

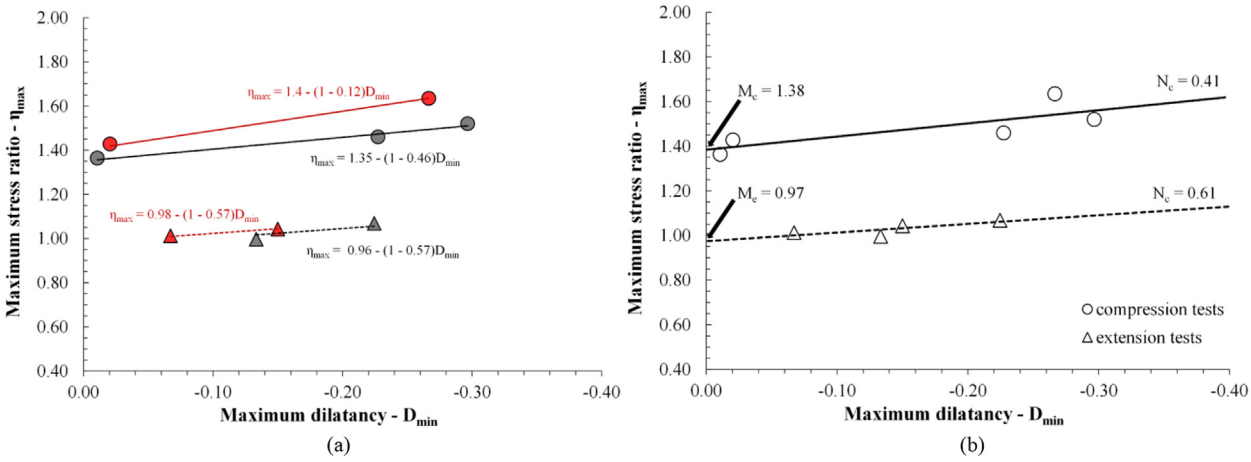

Fig. 13. Maximum stress ratio vs. maximum dilatancy considering (a) different fines contents and (b) compression and extension tests.

could not be determined in the present research as only two different gradings were tested. Also, Li and Coop (2019) suggested that a framework based on TFC might not be appropriate for tailings with natural gradings.

A similar tendency was observed for the extension tests with the CSL points shifting downwards with increasing fines content. The findings indicate that the flocks around the bulky particles (Fig. 6) possibly influence the volumetric behavior of the IOT specimens subjected to different stress paths. Furthermore, the higher amount of fines allows to achieve more compact arrangements locating the CSLs in ranges with smaller specific volumes in the v-lnp' plane.

4. Conclusions

An experimental study of two IOTs with different gradings was presented. The geotechnical behavior was analyzed by triaxial compression and extension tests under drained and undrained conditions. The main outcomes of the study are presented below.

(1) In the q-p' plane, the CSLs can be represented by straight lines for both compression and extension up to the stress level reached. For the finer tailings (S1), a gradient (M_c) of 1.4 was found (corresponding to a critical state friction angle $\varphi'_{cs} = 34.6°$) for compression and a gradient (M_e) of 0.98 ($\varphi'_{cs} = 35.8°$) for extension tests. The results for S2 (coarser tailings) were similar, indicating a slightly higher critical state friction angle for extension tests ($M_e = 0.97$ and $\varphi'_{cs} = 34.8°$) compared to compression tests ($M_c = 1.35$ and $\varphi'_{cs} = 33.4°$). Regarding the fines content, the studied tailings showed similar values for φ'_{cs} with the finer material presenting slightly higher strength in both compression and extension.

(2) Different values of M were obtained for compression and extension stress paths. This is associated with the relative magnitude of the intermediate principal stress in the extension tests in relation to compression tests. Intermediate principal stress equal to major principal stress (extension) imposes a more severe condition on the specimen and thus

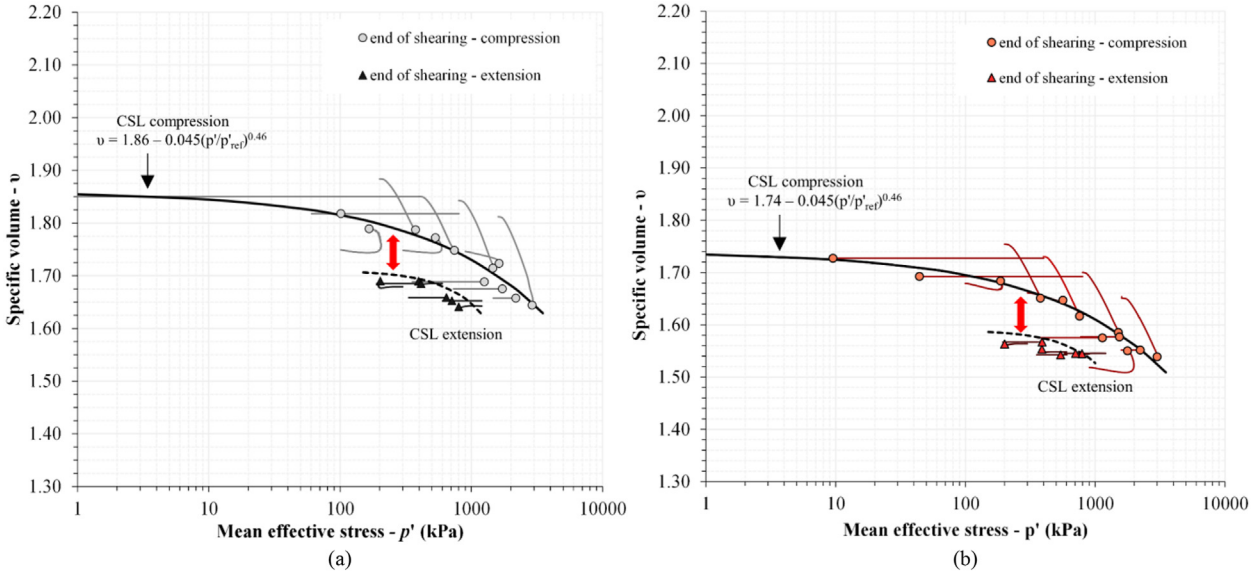

Fig. 14. CSLs in the v-lnp' plane for (a) S1 and (b) S2.

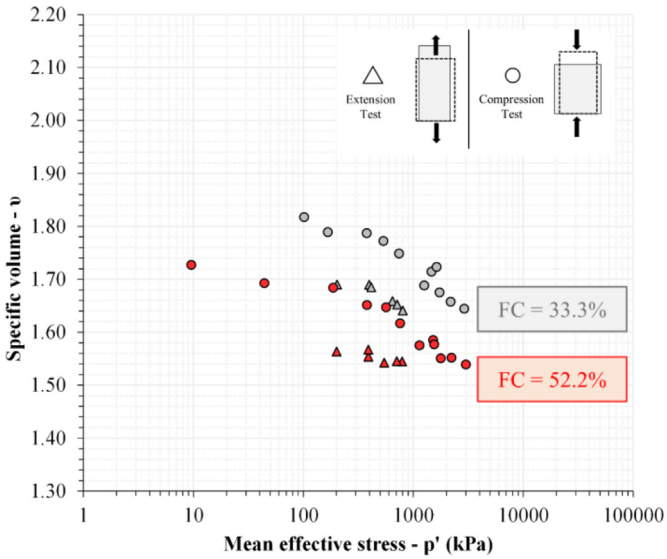

Fig. 15. Fines content influence on compression and extension tests.

reduces the stress ratio achieved by the shearing. However, the critical state friction angle is similar for compression and extension and this property is associated with strength mechanisms. The molding based on compaction, and application of specified energy in axial direction may give rise to a preferential particle orientation and consequent anisotropy. This effect, associated with greater confinement in extension tests, can increase the difficulty of particle rearrangement, favoring the development of different strain mechanisms in these tests, and thus increasing the mobilized frictional resistance between the grains.

(3) The maximum stress ratio (η_{max}) is proportional to the maximum dilatancy (D_{min}) for the two materials in compression and extension stress paths. A linear equation was fit for each case, and it is possible to obtain the respective M_c (or M_e) value at zero dilation. Different gradient values were obtained in the fits, especially between compression and extension tests, and can suggest the existence of non-unique CSLs for these materials. The tests did not show an evident influence of the different fines content on the dilatancy of the materials both in compression and extension.

(4) Curved stress path dependent CSLs were obtained for both tailings on plane in v-lnp'. Despite the lower strain reached, it is suggested that the location of CSL for extension tests does not converge to the CSL defined for compression tests. The stress–strain–dilatancy analysis performed supports the concept of multiple CSL. The offset from the CSL for compression tests is similar for S1 and S2, with the CSL defined for extension tests below the one defined in compression. One possible cause for the non-uniqueness in the v-lnp' plane is the deformation mode and strain direction that the specimen is subjected to. It is possible to suggest that the position of the CSL in the volumetric plane is more influenced by the strain path than the stress path of the tests.

(5) The curved CSLs obtained is not a feature of particle breakage. Particle size distribution analysis of tested specimens has not presented any indication of particle breakage during shearing for the stress levels considered. The existence of curved CSL is, thus, related to the existence of a region where the material can exist in a metastable state at low pressures, which gives rise to an undefined critical state in this region.

(6) It is demonstrated that fines content affects the extension and compression volumetric behavior of the tailings studied. The CSLs in the v-lnp' plane shift downwards with the increasing fines content for compression and extension tests. The findings indicate that the flocks around the bulky particles influence the volumetric behavior of the IOT specimens subjected to different stress paths.

(7) The mechanical behavior of IOTs concerns the volumetric behavior and shear strength, and it is found to be related directly to the shape of the grains and to the strain path followed during testing. This indicates that generalizations of critical states defined in compression to stress paths that account for different strain mechanisms should be carefully analyzed. Concerning the design of TSF, it is crucial to correctly determine the stress paths and the deformation mode that the material will be subjected to in the field during and after construction to provide adequate safety and serviceability to the executed structures. Furthermore, the influence of fines content on CSL indicates that a better understanding of the material in dense states, achievable due to the presence of smaller particles in the granular matrix, is still needed.

Declaration of competing interest

The authors declare that they have no known competing financial interests or personal relationships that could have appeared to influence the work reported in this paper.

Acknowledgements

The authors wish to express their appreciation to Vale S.A. and Brazilian Research Council (CNPq) for the support to the research group.

Notation

CSL	Critical state line
CSSM	Critical state soil mechanics
DEM	Discrete element method
FC	Fines content
IOT	Iron ore tailings
SEM	Scanning electronic microscope
TFC	Threshold fines content
TSF	Tailings' storage facilities
C_u	Coefficient of uniformity
C_c	Coefficient of curvature
D	Dilation rate (de_v/de_s)
D_{min}	Minimum dilation rate
e	Void ratio
e_{min}	Minimum void ratio
e_{max}	Maximum void ratio
G_s	Specific gravity
K	Horizontal to vertical effective stress ratio
M	Critical stress ratio
M_c	Critical stress ratio in triaxial compression
M_e	Critical stress ratio in triaxial extension
φ'_{cs}	critical state friction angle
g	Specific weight
v	Specific volume, and $v = 1 + e$
v_i	Specific volume prior to shearing
η	Stress ratio, and $\eta = q/p'$
η_{max}	Stress ratio at peak strength

p'	Mean effective stress
p'_0	Mean effective stress at the beginning of the shearing phase
q	Deviatoric stress, and $q = \sigma_1 - \sigma_3$
σ_1, σ_3	Principal stresses
σ'_1, σ'_3	Effective principal stresses
σ'_h	Horizontal effectives stress
σ'_a	Axial effective stress
ε_a	Axial strain
ε_v	Volumetric strain
w	Water content
Ψ	State parameter

References

ASTM D854–14, 2014. Standard Test Methods for Specific Gravity of Soil Solids by Water Pycnometer. ASTM International, West Conshohocken, USA.

ASTM D7181–20, 2020a. Standard Test Method for Consolidated Drained Triaxial Compression Test for Soils. ASTM International, West Conshohocken, USA.

ASTM D4767–11(2020), 2020b. Standard Test Method for Consolidated Undrained Triaxial Compression Test for Cohesive Soils. ASTM International, West Conshohocken, USA.

ASTM D4318–17e1, 2017a. Standard Test Methods for Liquid Limit, Plastic Limit, and Plasticity Index of Soils. ASTM International, West Conshohocken, USA.

ASTM D2487–17e1, 2017b. Standard Practice for Classification of Soils for Engineering Purposes (Unified Soil Classification System). ASTM International, West Conshohocken, USA.

ASTM D7928–21e1, 2021a. Standard Test Methods for Particle-Size Distribution (Gradation) of Fine-Grained Soils Using the Sedimentation (Hydrometer) Analysis. ASTM International, West Conshohocken, USA.

ASTM D698–12, 2021b. Standard Test Methods for Laboratory Compaction Characteristics of Soil Using Standard Effort, 12,500 ft-lb/ft^3 (600 kN-m/m^3). ASTM International, West Conshohocken, USA.

ASTM D1557–12, 2021c. Standard Test Methods for Laboratory Compaction Characteristics of Soil Using Modified Effort (56,000 Ft-Lbf/ft^3 (2,700 kN-M/m^3)). ASTM International, West Conshohocken, USA.

Atkinson, J.H., 2007. The Mechanics of Soils and Foundations, second ed. Taylor & Francis, London, UK.

Been, K., Jefferies, M.G., Hachey, J., 1991. The critical state of sands. Geotechnique 41 (3), 365–381.

Carrera, A., Coop, M.R., Lancellotta, R., 2011. Influence of grading on the mechanical behaviour of Stava tailings. Geotechnique 61 (11), 935–946.

Chu, J., 1995. An experimental examination of the critical state and other similar concepts for granular soils. Can. Geotech. J. 32 (6), 1065–1075.

Corrêa, M.M., Oliveira Filho, W.L., 2019. Impact of methods used to reconstitute tailings specimens on the liquefaction potential assessment of tailings dams. REM Int. Eng. J. 72 (3), 507–513.

Davies, M., 2011. Filtered dry stacked tailings: the fundamentals. In: Proceedings of the Tailing and Mine Waste Conference 2011. The University of British Columbia, Vancouver, Canada.

Fotovvat, A.R., Sadrekarimi, A., 2022. Instability of a gold mine tailings subjected to different stress paths. J. Geotech. Geoenviron. Eng. 148 (5), 04022020.

Fourie, A.B., Blight, G.E., Papageorgiou, G., 2001. Static liquefaction as a possible explanation for the Merriespruit tailings dam failure. Can. Geotech. J. 38 (4), 707–719.

Frost, J., Park, J.Y., 2003. A critical assessment of the moist tamping technique. Geotech. Test J. 26 (1), 57–70.

Gao, Z., Zhao, J., Li, X.S., Dafalias, Y.F., 2014. A critical state sand plasticity model accounting for fabric evolution: sand model accounting for fabric evolution. Int. J. Numer. Anal. Methods GeoMech. 38 (4), 370–390.

Huang, X., Hanley, K.J., O'Sullivan, C., Kwok, C.Y., Wadee, M.A., 2014. DEM analysis of the influence of the intermediate stress ratio on the critical-state behaviour of granular materials. Granul. Matter 16, 641–655.

Jefferies, M., Been, K., 2015. Soil Liquefaction: A Critical State Approach, second ed. CRC Press, London, UK.

Jefferies, M.G., Shuttle, D.A., 2002. Dilatancy in general Cambridge-type models. Geotechnique 52 (9), 625–638.

Kang, X., Xia, Z., Chen, R., Ge, L., Liu, X., 2019. The critical state and steady state of sand: a literature review. Mar. Georesour. Geotechnol. 37 (2), 1105–1118.

Kodicherla, S.P.K., Gong, G., Fan, L., Wilkinson, S., Moy, C.K.S., 2021. Discrete element modelling of strength and critical state characteristics of granular materials under axial compression and axial extension stress path tests. Particuology 56, 152–162.

Ladd, R., 1978. Preparing test specimens using undercompaction. Geotech. Test J. 1 (1), 16–23.

Li, G., Ovalle, C., Dano, C., Hicher, P.Y., 2013. Influence of grain size distribution on critical state of granular materials. In: Yang, Q., Zhang, J.M., Zheng, H., Yao, Y. (Eds.), Constitutive Modeling of Geomaterials. Springer, Berlin/Heidelberg, Germany, pp. 207–210.

Li, W., Coop, M.R., 2019. The Mechanical behaviour of Panzhihua iron tailings. Can. Geotech. J. 56 (3), 420–435.

Li, W., Coop, M.R., Senetakis, K., Schnaid, F., 2018. The mechanics of a silt-sized gold tailing. Eng. Geol. 241, 97–108.

Li, X.S., Dafalias, Y.F., 2012. Anisotropic critical state theory: role of fabric. J. Eng. Mech. 138 (3), 263–275.

Lupo, J., Hall, J., 2011. Dry stack tailings – design considerations. In: Tailings and Mine Waste'10: Proceedings of the 14th International Conference on Tailings and Mine Waste. CRC Press, London, UK.

Matsuoka, H., Nakai, T., 1974. Stress-deformation and strength characteristics of soil under three different principal stresses. Proc. Japan Soc. Civil Eng. 1974 (232), 59–70.

Mooney, M.A., Finno, R.J., Viggiani, M.G., 1998. A unique critical state for sand? J. Geotech. Geoenviron. Eng. 124 (11). https://doi.org/10.1061/(ASCE)1090-0241(1998)124:11(1100).

Riemer, M.F., Seed, R.B., 1997. Factors affecting apparent position of steady-state line. J. Geotech. Geoenviron. Eng. 123 (3), 281–288.

Salvatore, E., Modoni, G., Andò, E., Albano, M., Viggiani, G., 2017. Determination of the critical state of granular materials with triaxial tests. Soils Found. 57 (5), 733–744.

Schnaid, F., Bedin, J., Viana da Fonseca, A.J.P., Costa Filho, L.M., 2013. Stiffness and strength governing the static liquefaction of tailings. J. Geotech. Geoenviron. Eng. 139 (12), 2136–2144.

Schofield, A., Wroth, C.P., 1968. Critical State Soil Mechanics. McGraw-Hill, New York, USA.

Sladen, J.A., Handford, G., 1987. A potential systematic error in laboratory testing of very loose sands. Can. Geotech. J. 24 (3), 462–466.

Thevanayagam, S., Shenthan, T., Mohan, S., Liang, J., 2002. Undrained fragility of clean sands, silty sands, and sandy silts. J. Geotech. Geoenviron. Eng. 128 (10), 849–859.

Torres-Cruz, L.A., Santamarina, J.C., 2020. The critical state line of nonplastic tailings. Can. Geotech. J. 57 (10), 1508–1517.

Verdugo, R., Ishihara, K., 1996. The steady state of sandy soils. Soils Found. 36 (2), 81–91.

Viana da Fonseca, A., Cordeiro, D., Molina-Gómez, F., 2021. Recommended procedures to assess critical state locus from triaxial tests in cohesionless remoulded samples. Geotechnics 1 (1), 95–127.

Yamamuro, J.A., Lade, P.V., 1996. Drained sand behavior in axisymmetric tests at high pressures. J. Geotech. Eng. 122 (2), 109–119.

Yoshimine, M., Ishihara, K., Vargas, W., 1998. Effects of principal stress direction and intermediate principal stress on undrained shear behavior of sand. Soils Found. 38 (3), 179–188.

Zhao, J., Guo, N., 2013. Unique critical state characteristics in granular media considering fabric anisotropy. Geotechnique 63 (8), 695–704.

Prof. Nilo Cesar Consoli is presently working as Scientist/Professor at Graduate Program in Civil Engineering at Universidade Federal University do Rio Grande do Sul (UFRGS), Brazil. He is a Scientist listed among the 1% most influential in the world according to studies developed in September 2022 by Stanford University, USA. He is innovation consultant for VALE (Brazilian Mining Company) e PETROBRAS (Brazilian Oil Company). He obtained his PhD degree in Civil Engineering at Concordia University, Canada in 1991, carried out postdoctoral research at University of Oxford (1996) and The University of Western Australia (2006). He is Associate Editor (AE) of ASCE *Journal of Geotechnical and Geoenvironmental Engineering*, ASCE *Journal of Materials in Civil Engineering*, *Geotechnical and Geological Engineering*, and *Proceedings of ICE/UK – Ground Improvement*. He also is Editorial Board Member of *Canadian Geotechnical Journal*, *Geosynthetics International* (ICE-UK), *Transportation Geotechnics* and *Indian Geotechnical Journal*. He was awarded with Telford Prize (2001) and Telford Premium (2009) by The Institution of Civil Engineers, UK. Prof. Consoli has published 241 peer-reviewed papers indexed in Scopus (7299 citations and *h*-index = 47). He is author of the book "*Pathology of Foundations*" published in 2015. Prof. Consoli has experience in Geotechnical and Geoenvironmental Engineering and Sustainability, acting on the following subjects: laboratory and field testing for the development of new geomateriais, mine tailings stacking, geopolymers, three pillars of sustainability, constitutive modeling and numerical simulation of special earthworks, artificially cemented soils, and reuse of industrial residues for soil stabilization.